Journal of Materials Chemistry A

Accepted Manuscript

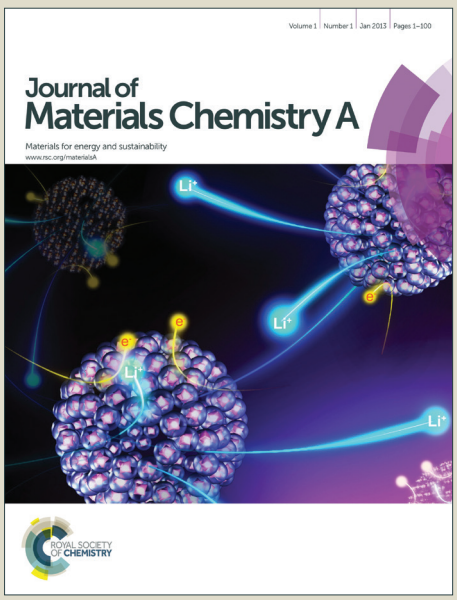

ROYAL SOCIETY OF CHEMISTRY

www.rsc.org/materialsA

Cite this: DOI: 10.1039/c0xx00000x

www.rsc.org/xxxxxx

ARTICLE TYPE

Enhanced photocatalytic activities by net-like hematite nanoparticle/graphene oxide composite†

Huanming Zhang,[a, b] Chunling Zhu,[b] Yujin Chen,*[a] Min Yang,[c] Piaoping Yang,*[b] Xiaohong Wu,*[c] Lihong Qi[a] and Fanna Meng[a,d]

Received (in XXX, XXX) Xth XXXXXXXXX 20XX, Accepted Xth XXXXXXXXX 20XX
DOI: 10.1039/b000000x

A facile strategy was developed to fabricate net-like hematite nanoparticle/graphene oxide (GO) composite (NHG), in which oxidization degree of GO could be controlled by simply changing annealing time. NHG with GO of appropriate oxidization degree and content exhibited much higher photocatalytic activities than those of α-Fe_2O_3 nanorods and commercial α-Fe_2O_3.

The direct conversion of sunlight into chemical fuels has been extensively studied due to significantly increasing demand of energy supply. α-Fe_2O_3 is a very promising material for photocatalytic water splitting because it possesses some attractive features such as favorable optical band gap (approximately 2.1 eV), chemical stability, nontoxicity and natural abundance. However, the sluggish reaction kinetics, short carrier lifetime and great shorter diffusion length of hole compared with the absorption depth lead to its poor photoelectrochemical (PEC) properties.[1-3] To make the photoinduced electron and hole separate effectively, some novel α-Fe_2O_3 nanostructures have recently been designed.[4,5] For example, hollow spheres composed of ultrathin α-Fe_2O_3 nanosheets with an average thickness of around 3.5 nm were synthesized, which showed a high photocatalytic activity for water oxidation.[4]However, the slow surface reaction kinetics need to be further improved. The introduction of closed shell ions (Al^{3+}, Sn^{4+}, and Si^{4+}) can address the issue efficiently, as previously reported.[6,7]

Recently, some graphene-based nanocomposites exhibited enhanced photocatalytic performance compared with single counterpart due to the large surface area and the platform structure of graphene.[8-10] On one hand, although monolayer graphene absorbs about 2.3% of visible light,[11] due to van der Waals force it is easy to restack to appear black, and consequently most of visible light will be absorbed by restacked graphene sheets, which will decrease the light absorption of the photocatalysts and then lower the photocatalytic performance of the graphene-based nanocomposites to some extent.[9] On the other hand, graphene (G) has electronic properties like metal with the work function of about 4.42 eV,[12] and thus the types of semiconductors loaded on the graphene surface for photocatalytic applications are highly restricted from the viewpoint of energy level matching.

Recent researches demonstrated that if graphene was oxidized appropriately, it could be transformed from a conductor to a semiconductor.[13]The band gap value of GO depends on its oxidization degree, and thus it has been tested as a photocatalyst for water splitting.[14] Significantly, the tunable band gap value of GO further extend its photocatalytic applications. For example, when incorporated with wide-band gap TiO_2, GO can serve as a sensitizer, whereas when incorporated with narrow-band gap g-C_3N_4 it can work as an electron sink.[15] Nevertheless, the optimal design of GO-based photocatalyst for water oxidization is still a challenging task.

It has been demonstrated that the morphology and the size of catalysts have an important effect on their photocatalytic properties.[16]α-Fe_2O_3 nanostructures with various morphologies have been prepared, such as nanoparticles, nanorods, nanotubes, nanoflakes, hollow nanospheres, nanocages, nanohorns, and colloidal nanocrystal clusters.[17] But so far synthesis and photocatlytic property of net-like hematite nanoparticle/graphene oxide composite (NHG) has not been reported. Herein we developed a facile method to fabricate NHG, in which oxidization degrees of GO could be controlled by simply changing annealing time. The net-like composite with GO of appropriate oxidization degree and content exhibited higher photocatalytic water oxidation rate (150 μmol $h^{-1}g^{-1}$) and much better PEC performance (0.86 mA/cm^2 at 1.6 V vs reversible hydrogen electrode (RHE)) than those of commercialα-Fe_2O_3 and α-Fe_2O_3 nanorods. The mechanism of such enhancement is discussed in detail.

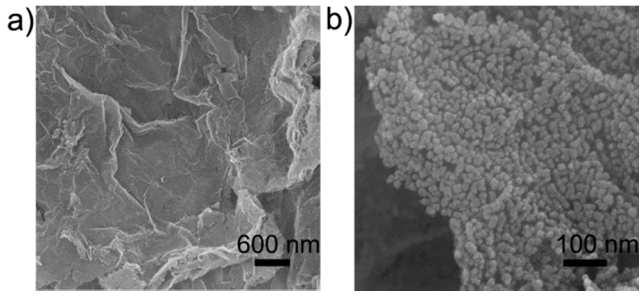

Fig. 1 SEM image of NHG, b) magnified-view of a).

The preparation of NHG (see Experimental section for details in Electronic Supplementary Information (ESI)) involved two steps.† G/β-FeOOH nanocomposites were first synthesized by

our previously reported method with a modification.[18]

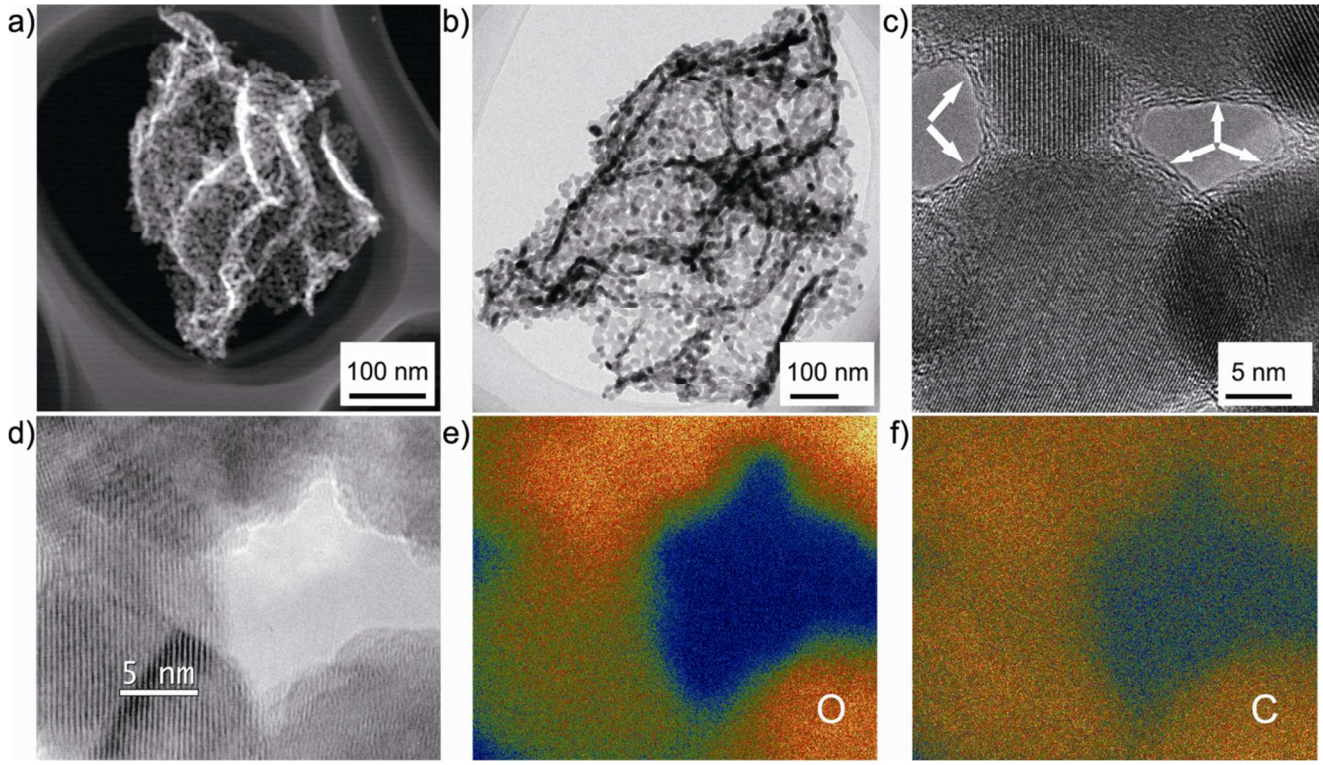

Fig.2 Characterization of NHG2 modified with GO: a) Dark field TEM image, b) TEM image, c), d) HRTEM images EDX elemental mappings of e) oxygen and f) carbon.

After annealing G/β-FeOOH nanocomposites at 500°C for 1 h at an air atmosphere, the net-like composite could be obtained simply. The color of the annealed sample is red rather than black (Fig. S1), and thus the influence of the light absorption by graphene on photocatalytic performance can be eliminated. † For convenience, the samples obtained at 500°C for 0.5, 1, and 2 h are named as NHG1, NHG2, and NHG3, respectively.

The scanning electron microscopy (SEM) and transmission electron microscopy (TEM) images of G/β-FeOOH nanocomposites show that the β-FeOOH clusters with a size of about 20 nm are distributed densely on the graphene sheets (Fig. S2). †A low-magnification SEM image of NHG2 clearly shows that the sample still remains graphene-like morphology (Fig. 1a), and the magnified SEM image shows that the net-like composite consists of small α-Fe_2O_3 particles with an average diameter of 15 nm. The X-ray diffraction (XRD) confirms the nanoparticles are rhombohedral α-Fe_2O_3 crystal (Fig.S3). † GO is not detected by XRD, which is attributed to its very small amount in the sample. In addition, NHG1 and NHG3 have a similar morphology as shown in Fig. S4. †

The net-like composite, composed of nanoparticle subunits, are further confirmed by TEM and annular dark-field (ADF) scanning transmission electron microscopy (STEM) images, as shown in Fig. 2a and 2b. Interestingly, we can find that some α-Fe_2O_3 nanoparticles are coated with graphene-like materials indicated by the arrows in the high-resolution TEM image (Fig. 2c and Fig. S5). It arises from inadequate combustion of graphene in G/β-FeOOH nanocomposites at an air atmosphere. Fig. 2d-f show ADF STEM and EDX elemental mappings of α-Fe_2O_3 nanoparticles. It can be found that the C element distributes mainly in the whole region of the α-Fe_2O_3 nanoparticles, which further confirms that the graphene-like materials cover over α-Fe_2O_3 nanoparticles'surface. The coating layers may be GO because the annealing process was carried out at 500°C at an air atmosphere.

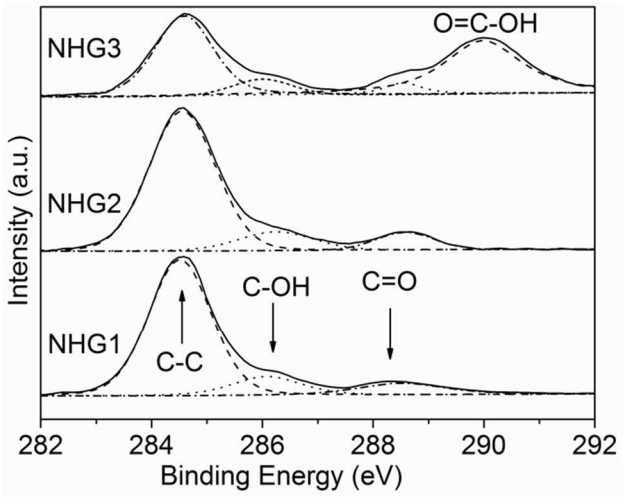

Fig. 3 High-resolution C1s spectrum of NHGs.

In order to verify this assumption, X-ray spectroscopy (XPS) was carried out to analyze the composition of the oxygen functional groups of the samples. Fig. 3 shows high-resolution C1s spectra of NHGs. There are three peaks, corresponding to C–C, C–OH, and C=O, in the C 1s spectra of NHG1 and NHG2. However, the intensity ratio of C–OH to C–C increases slightly from 0.13 in NHG1 to 0.136 in NHG2. Furthermore, the intensity ratio of C=O to C–C increases remarkably from 0.079 in NHG1 to 0.131 in NHG2. Thus, GO in HNG2 exhibits higher oxidization degree than that in NHG1. Besides these three peaks, in C 1s spectrum of NHG3 an additional peak at 289.5eV appears, which is assigned to O=C–OH functional groups.[19] Furthermore, the intensities of the C–OH and C=O peaks in C 1s spectrum of NHG3 increased further compared with those of NHG1 and NHG2. These results above proved that the residual graphene in the samples has been oxidized and the oxidization degree depends on annealing time. The GO contents in the samples were determined to be about 6.7, 5.6 and 1.6 wt% in NHG1, NHG2, and NHG3, respectively, by inductively coupled plasma (ICP) mass spectrometry.†

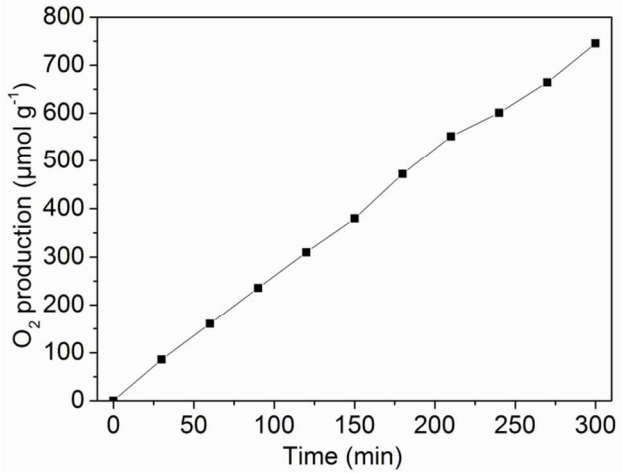

Fig. 4 O_2 evolution from NHG2 with $Na_2S_2O_8$as electron sacrifice reagent.

UV-vis absorbance spectra are shown in Fig. S6a. NHG2 and NHG3 exhibited an absorption edge at 585 nm, whereas NHG1 showed an absorption edge at 596 nm.† The Tauc plots of NHGs for an indirect transition with band gap of about 2.1 eV and a direct transition with band gap of about 2.17 eV are shown in Fig. S6c and d, respectively. [20a] According to the equation, $\alpha h\nu = A(h\nu - E_g)^n$ (n is 0.5 for a direct and 2 for an indirect transition), we gave $\alpha h\nu$ *vs* ($h\nu - E_g$) curves, as shown in Fig. S6b. The slope (n) is about 1.9, close to 2, indicating an indirect transition in NHGs.[2a]† The slight smaller band gap value of NHG1 may result from residual lattice strain caused by relatively shorter annealing time. As all the peaks of NHG1 in XRD are slightly shifted towards a lower angle, and the peak corresponding to (104) with an angle shift of 0.1° was taken for example (Fig. S7), but this was not observed in other samples. †According to Bragg's law: $n\lambda=2d\sin\theta$, where n is an integer, λ is the wavelength of incident wave, d is the spacing between the planes in the atomic lattice, and θ is the angle between the incident ray and the scattering planes. The smaller θ leads to the lager d, which means the enlarged lattice constants. This was proved by the larger lattice parameters than standard values in Table. S1. † Since band gap is inversely proportional to the product of lattice constants,[20b] NHG1 has slightly smaller band gap value.

The photocatalytic activities of NHGs, α-Fe_2O_3 nanorods, and commercial α-Fe_2O_3 were tested using $Na_2S_2O_8$ as electron sacrifice reagent.[21] For comparison, the photocatalytic activity of α-Fe_2O_3 nanorods with diameter of 50 nm (Fig. S8a) and commercial α-Fe_2O_3 (Fig. S8b) were also tested.† α-Fe_2O_3 nanorods were prepared according to previous report.[17b] From Fig. S9, the photocatalytic activities of the tested samples are in order: NHG2>NHG3>α-Fe_2O_3 nanorods>NHG1>commercial α-Fe_2O_3. † The poor activity of commercial α-Fe_2O_3 can be attributed to its large size and low surface area. The oxygen production rate of α-Fe_2O_3 nanorods is 110 μmol $h^{-1}g^{-1}$, lower than those of NHG2 (150 μmol $h^{-1}g^{-1}$, shown in Fig. 4). In addition, the net-like composites obtained at different annealing times exhibited different photocatalytic performance. As shown in Fig. S9, both NHG1 (85 μmol $h^{-1}g^{-1}$) and NHG3 (130 μmol $h^{-1}g^{-1}$) show lower oxygen production rate than NHG2. These results above reveal that both amount and oxidization degree of GO in NHG play very important roles in the photocatalytic water oxidization process. The excess and inadequate oxidization degree of GO would suppress photocatalytic water oxidization performance of NHGs.

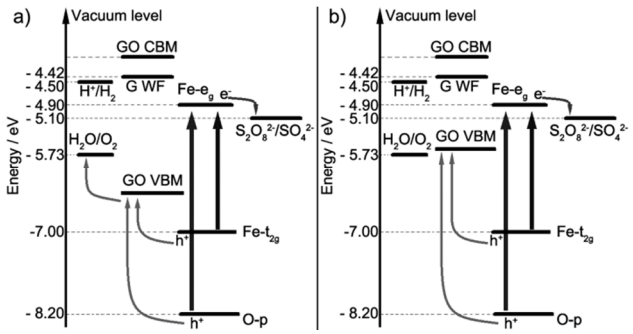

Fig. 5 Energy level diagram for hematite/G/GO, (a) VBM of GO crosses the oxidation potential of water, (b) VBM of GO below the oxidation potential of water.

The poor activity of commercial α-Fe_2O_3 can be attributed to its large size and low surface area. NHG2 has a lower specific surface area (41.7 m^2g^{-1}) than that of α-Fe_2O_3 nanorods (49.9 m^2g^{-1}), as shown in Fig. S10, but shows better performance.† Thus, the superiority in photocatalytic performance of NHG2 to α-Fe_2O_3 nanorods is not related to specific surface areas. In order to explore the cause of the enhancement in photocatalytic activities of NHG2, energy level diagrams for α-Fe_2O_3, G, and GO are plotted, as shown in Fig. 5, based on the literature value of the conduction band edge (E_{CB}) = + 0.40 V vs normal hydrogen electrode (NHE) for hematite at pH 7,[22] and the optical band gaps for the d-d and ligand-to-metal charge transfer (LMCT) transitions. Holes for oxygen evolution can be generated either by visible light excitation (Fe-t_{2g} orbital) or by UV excitation (O-p band),[23] as shown in Fig. 5.

Since the valence and conduction bands of graphene, consisting of bonding π and anti-bonding π (π*) orbitals, respectively, touch at the Brillouin zone corners, which makes a

single sheet of graphene a zero band-gap semiconductor.[24] However, introducing oxygen-containing groups would remove the equivalence of the two carbon sublattices in graphene by forming C–O covalent bonds that damage the original orbitals. It would result in separation of damaged π and π* orbitals and create a band gap in graphene.[13]If more oxygen is introduced, the band gap would further enlarged, and the valence band maximum (VBM) would gradually change from the π orbital of graphene to the 2p orbital of oxygen; however, the π* orbital remains as the conduction band minimum (CBM).[13]

Fig. 5a and b show energy level diagrams corresponding to high and low oxidization degree of GO in net-like composite, respectively. Because the work function of graphene is 4.42 eV,[12] and the reported CBM of GO is about 4 eV,[14b] it is reasonable to presume that the CBM of the GO in NHGs is in range of 4-4.42 eV, depending on the oxidization degree of the graphene. CBM of GO is located above the NHE, while the CBM of Fe_2O_3 is under the NHE, therefore it's impossible for the photoinduced electrons of α-Fe_2O_3 to transfer to the CB of GO. Namely, GO doesn't play the role of electron collector and transporter to separate photoinduced electron-hole pairs, which is much different from previous reports on GO as an electron sink enhancing photocatalytic performance.[25a]

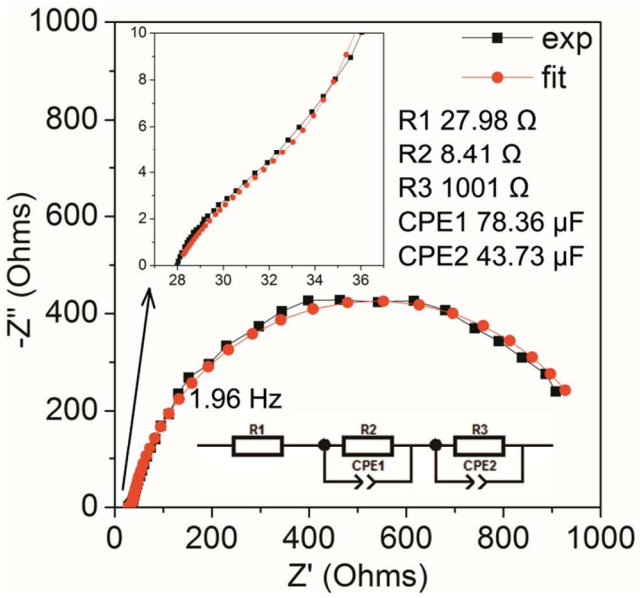

Fig. 6 a) EIS of NHG2, and insets showing the magnified-view of high frequency signals, corresponding equivalent circuit model and values of the elements in the model, respectively.

Thus, the only possible reason of higher photocatalytic performance of NHG2 is that the photoinduced holes can transfer from VBM of α-Fe_2O_3 to that of GO, as shown in Fig 5a. This assumption can be supported by electrochemical impedance spectroscopy (EIS) in Fig. 6a. There are two semicircles in the EIS of NHG2, of which one is located at low frequency signals and the other is located at high frequency signals. This means a two-step charge-transfer process mediated via surface states or reaction intermediates.[26a] The results could be well fitted with the equivalent circuit model in the inset of Fig. 6. Constant phase element (CPE) is an equivalent electrical circuit component that models the behavior of an electrical double layer, but not a perfect capacitor. R_3 corresponds to the charge transfer resistance, and the characteristic frequency of the active interfaces is 1.96 Hz, which may correspond to the hole injection rate.[26b] In contrast, two semicircles don't appear in the EIS of α-Fe_2O_3 nanorods (Fig. S11).† Fundamentally, the speed of holes injection into water is very slow for α-Fe_2O_3,[1] but fast for GO.[14b] Also, due to the serious surface recombination, the lifetimes of photogenerated holes in α-Fe_2O_3 are extremely short,[2b] while relatively long in GO.[25b]As a result, GO can serve as the reaction interface where holes inject into water to speed up oxygen evolution rate. Therefore, NHG2 showed better photocatalytic activity than α-Fe_2O_3.

Although oxidization degree of GO in NHG3 is higher than that of GO in NHG2, the GO content in NHG3 is much lower than that of GO in NHG2, leading to the poorer photocatalytic performance of NHG3. According to the XPS results, GO in NHG1 exhibits the lowest oxidization degree due to its shortest annealing time, suggesting the smallest band gap of GO in NHG1, as shown in Fig. 5b. In this case, VBM of GO is located above the oxidation potential of water. Because the photoinduced holes transferred from α-Fe_2O_3 to VBM of GO recombine with the photoinduced electrons of GO, the oxygen evolution rate of NHG1 decreases, even lower than that of α-Fe_2O_3 nanorods. In addition, the morphology of the net-like composite was well maintained without any change after the photocatalytic water oxidation test (Fig. S12), implying a good stability of such nanostructures as photocatalysts. †

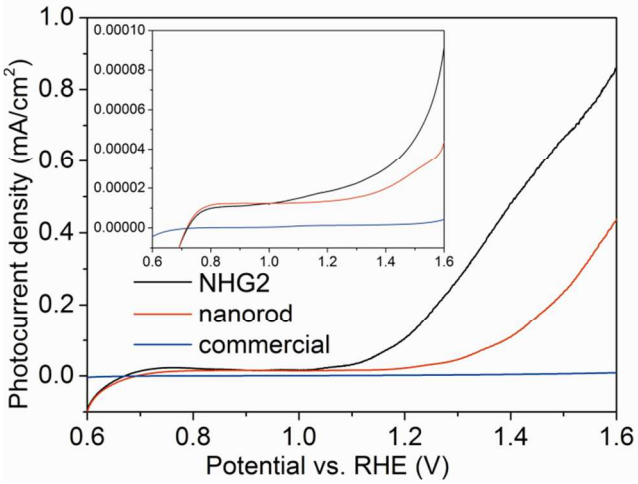

Fig. 7 PEC properties of NHG2, α-Fe_2O_3 nanorod, and commercial α-Fe_2O_3, and inset showing the dark currents of the different samples.

PEC properties of NHG2, α-Fe_2O_3 nanorods, and commercial α-Fe_2O_3 were also tested, as shown in Fig. 7. As expected, commercial α-Fe_2O_3 exhibits a negligible photocurrent density at 1.6 V vs RHE (0.009 mA/cm^2). A maximum photocurrent density of 0.86 mA/cm^2 at 1.6 V vs RHE was achieved by NHG2, significantly larger than that of α-Fe_2O_3 nanorods (0.43 mA/cm^2). Furthermore, NHG2 has lower onset potential (1.09 V vs RHE) than that of α-Fe_2O_3 nanorods (1.22 V vs RHE). Dark currents (inset of Fig 7) of NHG2 and nanorods are negligible because the

photocurrent densities under illumination are three orders of magnitudes larger than dark currents. Since the light harvesting efficiency is important when comparing the performance of different photoelectrodes, the absorption spectra were showed in Fig. S13. † There is no notable difference between NHG2 and nanorod photoelectrodes in the absorption spectra, except that nanorod photoelectrode shows slightly better absorption than NHG2 photoelectrode in UV region. Nanorods photoelectrode shows better absorption than NHG2 photoelectrode, but does worse in PEC performance. Thus, the large photocurrent density achieved by NHG is also attributed to the mechanism discussed above.

Conclusions

In summary, NHGs were prepared by a facile method. The oxidization degree of GO can be controlled by simply tuning annealing time. NHGs with GO of appropriately amount and oxidization degree exhibited much better photocatalytic water oxidation and PEC performance than those of α-Fe_2O_3 nanorods and commercial α-Fe_2O_3. The superiority is attributed to that the photoinduced holes can transfer from VBM of α-Fe_2O_3 to that of GO, and GO replaces with α-Fe_2O_3 as the reaction interface where holes inject into water to speed up oxygen evolution rate. Furthermore, the strategy presented here could be expended as a general method to synthesize other types of photocatalysts modified with GO for applications in water splitting.

Acknowledgments

We thank the National Natural Science Foundation of China (Grant no. 51272050, 51302047, 21203043 and 21271053), the National Science and Technology Support Program of China (Grant No. 2013BAE04B02), and also the 111 project (B13015) of Ministry Education of China to Harbin Engineering University.

Notes and references

[a]*Key Laboratory of In-Fiber Integrated Optics, Ministry of Education, College of Science, Harbin Engineering University, Harbin 150001, China, E-mail: chenyujin@hrbeu.edu.cn*
[b]*College of Materials Science and Chemical Engineering, Harbin Engineering University, Harbin 150001, China, E-mail: yangpiaoping@hrbeu.edu.cn*
[c]*School of Chemical Engineering and Technology, Harbin Institute of Technology, Harbin 150001, China, E-mail: wuxiaohong@hit.edu.cn*
[d]*Heilongjiang Institute of Science and Technology, Harbin 150027,China*
† Electronic Supplementary Information (ESI) available: Experimental detail and additional information. See DOI: 10.1039/b000000x/

1 M. D. Edwards, J. B. Goodenough, A. Hamnett and P. R. Trevellick, *J. Chem. Soc. Faraday Trans.*, 1983, **79**, 2027–2041.
2 a) J. H. Kennedy and K. W. Frese Jr, *J. Electrochem. Soc.*, 1978, **125**, 709–714; b) N. J. Cherepy, D. B. Liston, J. A. Lovejoy, H. M. Deng and J. Z. Zhang, *J. Phys. Chem. B*, 1998, **102**, 770–776.
3 R. F. G. Gardner, D. W. Tanner and F. Sweett, *J. Phys. Chem. Solids.*, 1963, **24**,1183–1186.
4 J. X. Zhu, Z. Y. Yin, D. Yang, T. Sun, H. Yu, H. E. Hoster, H. H. Hng, H. Zhang and Q. Y. Yan, *Energy Environ. Sci.*, 2013, **6**, 987–993.
5 T. K. Townsend, E. M. Sabio, N. D. Browning and F. E. Osterloh, *Energy Environ. Sci.*, 2011, **4**, 4270–4275.
6 a) J. A. Glasscock, P. R. F. Barnes, I. C. Plumb and N. Savvides, *J. Phys. Chem. C*, 2007, **111**, 16477–16488; (b) R. L. Spray, K. J. McDonald and K. S. Choi, *J. Phys. Chem. C*, 2011, **115**, 3497–3506.
7 I. Cesar , A. Kay , J. A. G. Martinez and M. Grätzel, *J. Am. Chem. Soc.*, 2006, **128**, 4582–4583.
8 W. G. Tu, Y. Zhou and Z. G. Zou, *Adv. Funct. Mater.*, 2013, **23**, 4996–5008.
9 Q. Li, B. D. Guo, J. G. Yu, J. R. Ran, B.H. Zhang, H.J. Yan and J. R. Gong, *J. Am. Chem. Soc.*, 2011, **133**, 10878–10884.
10 J. C. Meyer, A. K. Geim, M. I. Katsnelson, K. S. Novoselov, T. J. Booth and S. Roth, *Nature*, 2007, **446**, 60–63.
11 R. R. Nair, P. Blake, A. N. Grigorenko, K. S. Novoselov, T. J. Booth, T. Stauber, N. M. R. Peres and A. K. Geim, *Science*, 2008, **320**, 1308.
12 a) R. Czerw, B. Foley, D. Tekleab, A. Rubio, P. M. Ajayan and D. L. Carroll, *Phys. Rev. B*, 2002, **66**, 033408–033411; b) J. W. G. Wilder, L. C. Venema, A. G. Rinzler, R. E. Smalley and C. Dekker, *Nature*, 1998, **391**, 59–62; c) O Pellegrino, M R. Vilar, G. Horowitz and A. M. B. do Rego, *Mater. Sci. Eng. C*, 2002, **22**, 367–372.
13 J. Ito, J. Nakamura and A. Natori, *J. Appl. Phys.*, 2008, **103**, 113712–113716.
14 a) T. F. Yeh, J. M. Syu, C. Cheng, T. H. Chang and H. S. Teng, *Adv. Funct. Mater.*, 2010, **20**, 2255–2262; (b) T. F. Yeh, F. F. Chan, C. T. Hsieh and H. S. Teng, *J. Phys. Chem. C*, 2011, **115**, 22587–22597.
15 a) C. Chen,W. M. Cai,, M. C. Long,B. X. Zhou,Y. H. Wu,D. Y. Wu and Y. J. Feng, *ACS Nano*, 2010, **4**, 6425–6432; b) K. Dai, L. H. Lu, Q. Liu, G. P. Zhu, X. Q. Wei, J. Bai, L. L. Xuan and H. Wang, *Dalton Trans.*, 2014, **43**, 6295–6299.
16 A. R. Tao, S. Habas and P. D. Yang, *Small*, 2008, **4**, 310–325.
17 a) S. H. Sun, H. Zeng, D. B. Robinson, S. Raoux, P. M. Rice, Sh. X. Wang and G. X. Li, *J. Am. Chem. Soc.*, 2004, **126**, 273–279; b) C. J. Jia, L. D. Sun, Z. G. Yan, L. P. You, F. Luo, X. D. Han, Y. C. Pang, Z. Zhang and C. H. Yan, *Angew. Chem. Int. Ed.*, 2005, **44**, 4328–4333; c) J. Chen, L. N. Xu, W. Y. Li and X. L. Gou, *Adv. Mater.*, 2005, **17**, 582–586; d) M. V. Reddy, T. Yu, C. H. Sow, Z. X. Shen, C. T. Lim, G. V. SubbaRao and B. V. R. Chowdari, *Adv. Funct. Mater.*, 2007, **17**, 2792–2799; e) X. Lai, J. Li, B. A. Korgel, Z. Dong, Z. Li, F. Su, J. Du and D. Wang, *Angew. Chem. Int. Ed.*, 2011, **50**, 2738–2741; f) J. G. Yu, X. X. Yu, B. B. Huang, X. Y. Zhang and Y. Dai. *Cryst. Growth. Des.*, 2009, **9**, 1474–1480; g) Z. Y. Wang, D. Y. Luan, S. Madhavi, Y. Hu and X. W. Lou, *Energy Environ. Sci.*, 2012, **5**, 5252–5256; h) X. L. Fang, C. Chen, M. S. Jin, Q. Kuang,Z. X. Xie, S. Y. Xie, R. B. Huangand L. S. Zheng, *J. Mater. Chem.*, 2009, **19**, 6154–6160
18 a) Y. L. Ren, C. L. Zhu, S. Zhang, C. Y. Li, Y. J. Chen, P. Gao, P. P Yang and Q. Y. Ouyang, *Nanoscale*, 2013, **5**, 12296–12303; b) Y. L. Ren, H. Y. Wu, M. M. Lu, Y. J. Chen, C. L. Zhu, P. Gao, M. S. Cao, C. Y. Li and Q. Y. Ouyang, *ACS Appl. Mater. Interfaces*, 2012, **4**, 6436–6442.
19 D. X. Yang, A. Velamakanni, G. Bozoklu, S. Park, M. Stoller, R. D. Piner, S. Stankovich, I. Jung, D. A. Field, C. A. Ventrice Jr and R. S. Ruoff, *Carbon*, 2009, **47**, 145–152.
20 a) K. Sivula, R. Zboril, F. L. Formal, R. Robert, A. Weidenkaff, J. Tucek, J. Frydrych and Michael Grätzel, *J. Am. Chem. Soc.*, 2010, **132**, 7436–7444; b) R. Dalven, *Phys. Rev. B.*, 1973, **8**, 6033–6034.
21 F. A. Frame, T. K. Townsend, R. L. Chamousis, E. M. Sabio, T. Dittrich, N. D. Browning and F. E. Osterloh, *J. Am. Chem. Soc.*, 2011, **133**, 7264–7267.
22 Y. Xu and M. A. A. Schoonen, *Am. Mineral.*, 2000, **85**, 543–556.
23 L. A. Marusak, R. Messier and W. B. White, *J. Phys. Chem. Solids.*, 1980, **41**, 981–984.
24 C. Berger, Z. M. Song, X. B. Li, X. S. Wu, N. Brown, C. Naud, D. Mayou, T. B. Li, J. Hass, A. N. Marchenkov, E. H. Conrad, P. N. First and W. A. de Heer, *Science*, 2006, **312**, 1191–1196.
25 a) T. F. Yeh, J. Cihlář, C. Y. Chang, C. Cheng and H. S. Teng, *Mater Today*, 2013, **16**, 78–84; b) S. Kaniyankandy, S. N. Achary, S. Rawalekar and H. N. Ghosh, *J. Phys. Chem. C*, 2011, **115**, 19110–19116.
26 a) W. Gomes and D. Vanmaekelbergh, *Electrochim. Acta*, 1996, **41**, 967–973; b) C. Y. Cummings, F. Marken, L. M. Peter, K. G. U. Wijayantha and A. A. Tahir, *J. Am. Chem. Soc.*, 2012, **134**, 1228–1234.

Net-like hematite nanoparticle/graphene oxide composite, in which oxidization degree of graphene oxide can be controlled by simply tuning annealing time, exhibit highly photocatalytic performance for water splitting.